


CLINICAL ARTICLE

Application of CT-MRI Fusion-Based Three-Dimensional Reconstruction Technique in the Anatomic Study of Posterior Cruciate Ligament

Keyi Feng, MD^{1†}, Tianyue Wang, BD^{2†}, Jin Tang, MD¹, Xiaorui Hao, MD³, Xiaojun Ma, MD⁴, Zhenan Qu, MD⁴, Weiming Wang, PhD⁵ 

Department of ¹Bone and Joint Surgery and ²Maxillofacial Surgery, Chongqing University Three Gorges Hospital, Chongqing, ³Department of Orthopaedics, Nanping First Hospital affiliated to Fujian Medical University, Nanping and ⁴Department of Sports Medicine, Affiliated Zhongshan Hospital of Dalian University and ⁵Department of Sports Medicine, Affiliated Xinhua Hospital of Dalian University, Dalian, China

Abstract

Objective: During PCL reconstruction surgery, precise and personalized positioning of the graft tunnel is very important. In order to obtain patient-specific anatomical data, we established a three-dimensional knee joint fusion model to provide a unified imaging strategy, as well as anatomical information, for individualized and accurate posterior cruciate ligament (PCL) reconstruction.

Methods: This is an exploration study. From January 2019 to January 2020, 20 healthy adults randomly were enrolled and assessed via CT and MRI imaging. A three-dimensional fusion model of the knee joint was generated using the modified MIMIMICS and image fusion software. On the fused image, the areas of the femoral and tibial PCL footprint of both knees were measured. The anatomical center of the PCL footprint was measured at the femoral and tibial ends. The relevant bony landmarks surrounding the PCL femoral and tibial attachment were also measured. Paired *t*-tests were employed for all statistical analyzes, and $p < 0.05$ was considered as statistically significant.

Results: All 20 subjects achieved successful image fusion modeling and measurement, with an average duration of 12 h. The lengths of the LF1-LF3 were 32.1 ± 1.8 , 6.8 ± 2.5 , and 23.3 ± 2.1 mm, respectively. The lengths of the LT1-LT3 were 37.3 ± 3.3 , 45.6 ± 5.3 , and 6.0 ± 1.2 mm, respectively. The distances between the tibial PCL center of the left knee to the medial groove, champagne-glass drop-off, and the apex of the medial intercondylar were 8.4 ± 2.4 , 9.2 ± 1.8 , and 15.3 ± 1.4 mm, respectively, and the corresponding distances from the right knee were 8.0 ± 2.0 , 9.4 ± 2.2 , and 16.1 ± 1.8 mm, respectively. We observed no difference between the bilateral sides, in terms of the distance from the PCL center to the PCL attachment-related landmark, under arthroscopic guidance. The area of the femoral and tibial PCL footprints on the left knee were 115.3 ± 33.5 and 146.6 ± 24.4 mm², respectively, and the corresponding areas on the right knee were 121.8 ± 35.6 and 142.8 ± 19.5 mm², respectively. There was no difference between the bilateral sides in terms of the PCL footprint areas.

Conclusion: In the fusion image, the PCL attachment center and relevant bony landmarks which can be easily identified under arthroscopy can be accurately measured. The model can also obtain personalized anatomical data of the PCL on the unaffected side of the patient, which can guide clinical PCL reconstruction.

Key words: bony landmarks; CT-MRI fusion model; footprint area; posterior cruciate ligament; three-dimensional reconstruction technique

Address for correspondence: Weiming Wang, Department of Sports Medicine, Affiliated Xinhua Hospital of Dalian University, No.156, Wansui, Shahekou, Dalian, China. Email: 13594788835@163.com

[†]Keyi Feng and Tianyue Wang should be considered joint first author

Received 6 March 2022; accepted 5 August 2022



Introduction

The posterior cruciate ligament (PCL) originates from the lateral wall of the femoral medial condyle and inserts itself into the posterior half of the tibial PCL slope and the posterior angle of the lateral meniscus, which, in unison, maintains the posterior and rotational stability of the knee joint¹⁻⁴. Clinically, the primary complaint after acute PCL injury is pain, and it usually involves the patellofemoral, anteromedial, or posterior part of the knee, particularly during ascending and descending from stairs. However, the perception of instability becomes more apparent in chronic and combined PCL injuries. Joint instability occurs during the chronic phase of PCL injury. Hence, an appropriate intervention in the acute phase is crucial to the prevention of joint instability.

Currently, PCL reconstruction is the preferred intervention for PCL injury, carrying the advantages of native knee kinematics restoration, as well as prevention of residual posterior and combined rotatory knee laxity *via* an individualized approach^{5,6}. Although several surgical techniques are used to correct PCL injury, there is still a failure rate of 1%–25% after primary PCL reconstruction, and it even amounts to 45% if unfavorable patient-reported outcomes are regarded as subjective failures^{7,8}. Additionally, knee degeneration is not completely abolished, with incidences between 15%–60%^{9,10}. Thirty-three per cent of PCL reconstruction failures are due to improper tunnel placement, such as a more posterior placement of the femoral tunnel or a more proximal placement of the tibial tunnel¹¹. Studies revealed that the accurate anatomical positioning of the graft tunnel and proper restoration of the PCL anatomy are critical for good outcomes in arthroscopic-guided PCL reconstruction^{12,13}.

In clinical practice, arthroscopic direct vision and intraoperative fluoroscopy play key roles in the intraoperative anatomic positioning of arthroscopic PCL reconstruction¹⁴. Unfortunately, there is lack of a reliable approach of anatomical positioning, and, currently, it mostly depends on the surgeon's experience. Intraoperative fluoroscopic positioning mainly relies on prior imaging data, which is more in line with clinical needs than cadaveric measurement data^{15,16}. The anatomy of the PCL tibial end was extensively studied and described in several studies, using two-dimensional imaging techniques, such as plain radiographs, computed tomography (CT), and MRI^{17,18}. However, it is necessary to mark the PCL footprint area and center on the cadaver specimen in advance. Moreover, with the deepening of PCL anatomical research, it is also obvious that there are distinct individual differences in PCL anatomy. Thus, certain scholars proposed that the placement and evaluation of the graft tunnel must be guided by the personalized anatomical positioning of the PCL footprint area of patients¹⁹. To obtain patient-specific anatomical data, especially the shape, location, and alignment of the PCL insertion, imaging studies are still the best option. Recent studies reported the establishment of a three-dimensional fusion model of the knee joint, using MRI and CT, to directly obtain patient's personalized knee joint data²⁰. However, no publications employed this 3D technology to perform a detailed

quantitative investigation of PCL anatomy, the center of the footprint area, and PCL attachment-related bony landmarks.

In this study, the three-dimensional knee fusion model was established, using CT and MRI. Basic anatomical evaluation on PCL and bony landmarks surrounding the PCL were performed using this model. Our aim was to provide a unified and reliable anatomical landmark, using imaging anatomical information, to obtain preoperative simulated bone tunnel localization, which will ultimately guide personalized and accurate PCL reconstruction strategy.

Methods and Materials

Inclusion and Exclusion Criteria

The inclusion criteria were as follows: (i) patients aged between 20–40 years old; (ii) patients with normal knee joint and no obvious limb deformity; (iii) the PCL of included patients was intact and without damage; (iv) there was no fracture at the PCL attachment point; and (v) all voluntary patients signed an informed consent.

The exclusion criteria were as follows: (i) pregnant women; (ii) patients with a history of knee injury or surgery; (iii) patients with knee joint degenerative alterations, history of osteoarthritis, obvious deformity (varus and varus), or other knee joint injuries that may influence the resolution and measurement of PCL images; (iv) patients who were claustrophobic or mentally abnormal, and unable to manage their behaviors; and (v) patients who did not agree to undergo MRI and CT examinations.

General Information

This study recruited 20 healthy adults between January 2019 and January 2020, whose both knees were examined by CT and MRI. The procedures were reviewed and approved by the hospital ethics committee and were in accordance with the Declaration of Helsinki (No. 20190134), and all volunteers signed an informed consent form. There were 10 males and 10 females, with a mean age of 26.4 ± 1.6 years (range, 24–29 years). The mean height was 168.5 ± 6.5 cm (range, 159–178 cm), and the mean weight was 58.0 ± 6.0 kg (range, 49–67 kg). The research process of this article was shown in the flow chart (Figure 1).

Data Collection

All volunteers' knee joints were examined *via* MRI (Signa 3.0 T) and CT (64 Row CT). The scanning position of each subject was 0° – 15° of natural knee extension and external rotation, and the CT and MRI scans were performed within 30 min. The CT scan parameters were as follows: 120kV, automatic mA, scan time = 5s, full plain scan, matrix = 512×512 , window diameter = 360 mm, slice thickness = 1 mm, and reconstruction interval slice thickness = 1 mm. The fixed MRI machine used a head coil as the receiving coil, and the selection was made to scan the sagittal plane 3D proton density-weighted imaging sequence. The imaging scan parameters were as follows: TR (repetition time) = 11,000 ms, TE (echo time) = 25 ms; slice thickness = 1.2 mm; slice spacing = 1.2 mm; echo chains = 14; number of excitations

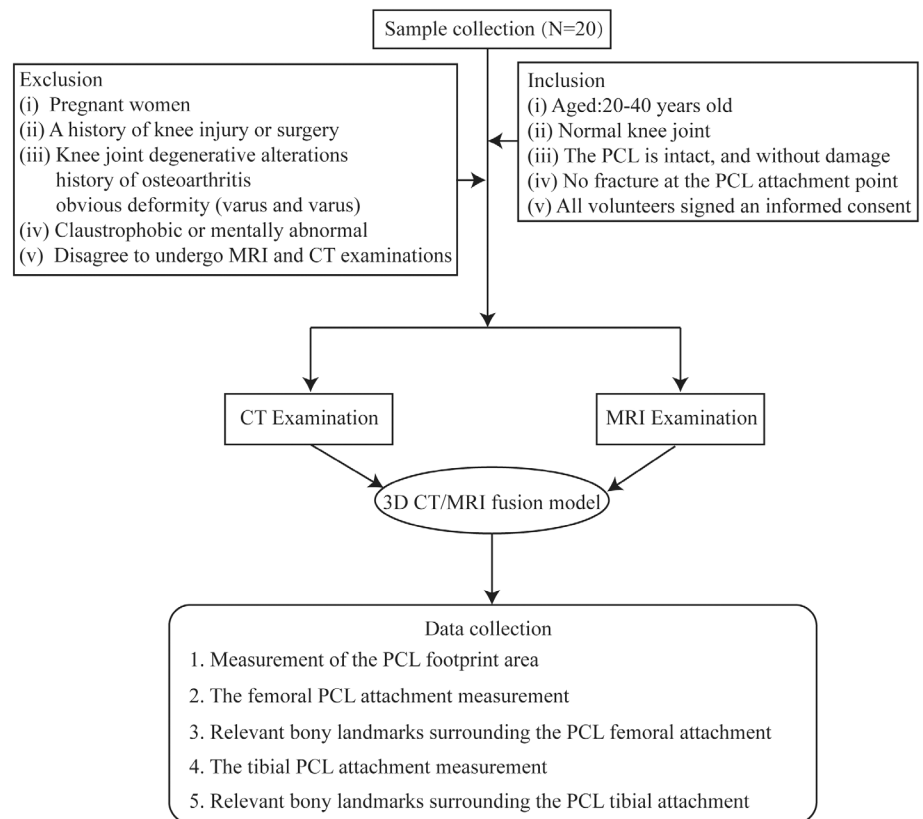


Fig. 1 The flow chart of the research process.

(NEX) = 2; matrix = 192/320; FOV = 18. Upon completion of imaging, the acquired MRI and CT scans were stored in CD-ROM using the DICOM format.

The Establishment of a 3D Knee Joint Fusion Model

The knee joint CT and MRI imaging data were next imported into Mimics 20.0 and the image fusion software (Readitec, China) for image segmentation and 3D reconstruction, respectively. The PCL-containing region at each MRI slice was automatically framed in Mimics 20.0 by setting a PCL boundary signal threshold. Then, the precise boundaries were delineated by an experienced senior clinician and a senior imaging professional doctor. The image was then imported into the image fusion software, combined with the CT image, to establish the 3D fusion model. We corrected this model by referencing common and obvious landmarks, such as, tibial tuberosity, tibial plateau, and so on. Eventually, a satisfied 3D fusion model was established, in which the tibia, femur, PCL, meniscus, and cartilage were clearly visualized, as shown in Figure 2A.

Data Measurement

Measurement of the PCL Footprint Area

The PCL footprint data was anatomically measured on the 3D fused image, using the measurement tool of the Mimics

software. The data included the area of the femoral and tibial PCL footprint of bilateral knees, as shown in Figure 2B–C.

The Femoral PCL Attachment Measurement

The distance from the center of the PCL to the medial border of the medial femoral condyle (LF1) was measured, and the percentage of the LF1 to the diameter of the femoral condyle (PF1) was calculated. Likewise, the vertical distance from the center of the PCL to the Blumensaat line (LF2) was measured carefully, and the percentage of LF2 to the distance from the Blumensaat line to the most distal edge of the medial femoral condyle (PF2) was also calculated. Lastly, the distance from the center of the PCL to the anterior cortex of the medial femoral condyle (LF3) was measured, and the percentage of the LF3 to the length of the Blumensaat line (PF3) was also calculated. A schematic diagram of these measurements is presented in Figure 3.

Measurement of Bony Landmarks Surrounding the PCL Femoral Attachment

The apex of the trochlear groove, superficial points, and posterior points were labeled, and the distance from these locations to the center of the PCL were measured (LF4, LF5, and LF6, respectively).

The superficial is the lowest points at the junctional edge between the lateral wall of the medial femoral condyle and the cartilage when the knee is straightened, and it is the

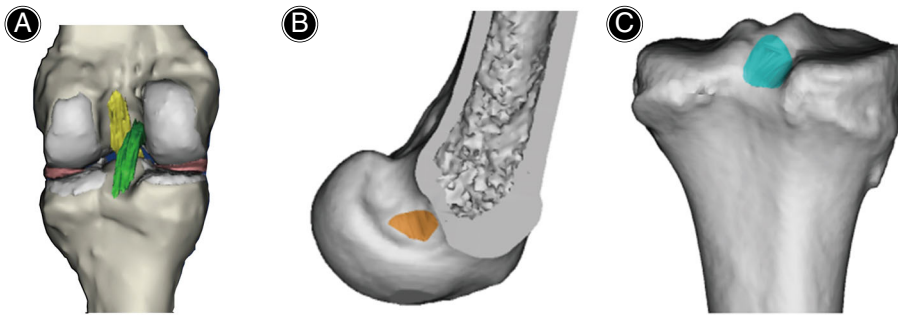


Fig. 2 (A) The diagram of 3D CT-MRI fusion model. The tibia, femur, PCL, meniscus, and cartilage are clearly visualized; (B) Femoral PCL footprint area; (C) Tibial PCL footprint area.

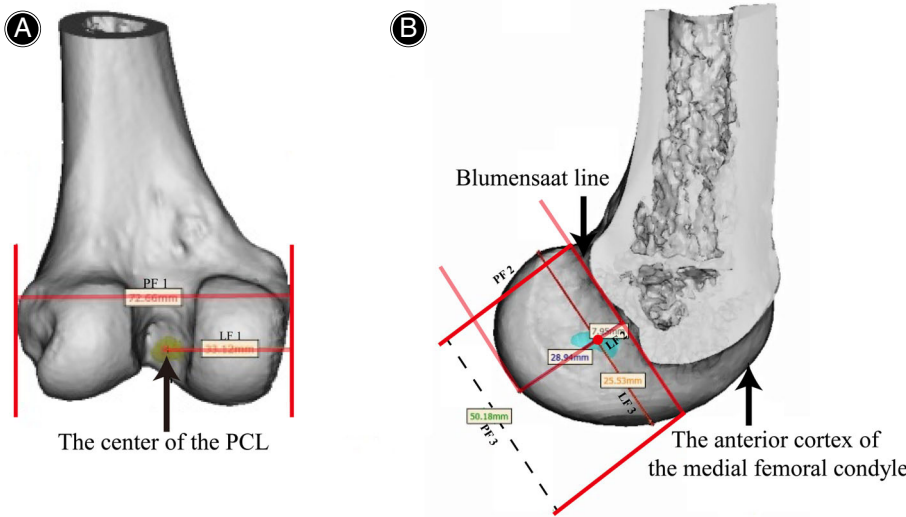


Fig. 3 Measurement of anatomical landmarks around the PCL femoral attachment: (A) LF1 represents the distance from the center of the PCL footprint to the medial border of the medial femoral condyle; PF1 represents the diameter of the femoral condyle. (B) LF2 represents the vertical distance from the center of the PCL footprint in femur to the Blumensaatt line; PF2 represents the distance from Blumensaatt line to the most distal edge of the medial femoral condyle; LF3 represents the distance from the center of the PCL footprint to the anterior cortex of the medial femoral condyle; PF3 represents the length of Blumensaatt line.

shallowest point at the junction edge between the lateral wall of the femoral medial condyle and the cartilage when the knee was flexed at 90°.

The posterior point, the most posterior point of the cartilage junction of the lateral wall of the femoral medial condyle in the straight position of the knee, is the lowest point of the cartilage junction of the lateral wall of the femoral medial condyle when the knee was flexed at 90°. A schematic diagram of these measurements is presented in Figure 4.

Measurement of the PCL Tibial Attachment

The distance from the PCL center to the medial edge of the tibial plateau (LT1) was measured, and the percentage of the LT1 to the width of the tibial plateau (PT1) was calculated. The distance from the PCL center to the anterior edge of the tibial plateau (LT2) was measured, and the percentage of the LT2 to the anterior and posterior diameters of the tibial plateau (PT2) were also calculated. The vertical distance from the PCL center to the lowest plane of the tibial plateau (LT3) was evaluated, and the percentage of the LT3 to the rotation angle of the tibial plateau to the medial tibial plateau (PT3) was calculated. A schematic diagram of these measurements is presented in Figure 5A–B.

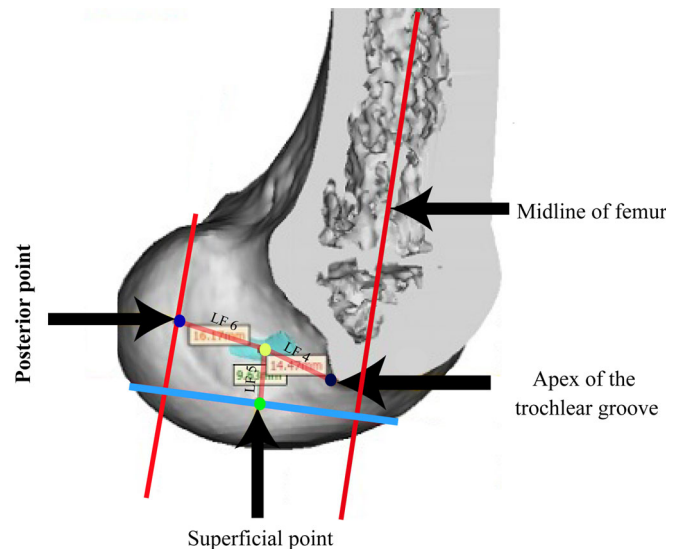


Fig. 4 The bony landmarks of PCL in the fusion images: LF4 represents the distance from apex of the trochlear groove to the center of PCL footprint in femur; LF5 represents the distance from superficial point to the center of PCL footprint in femur; LF6 represents the distance from posterior point to the center of PCL footprint in femur.

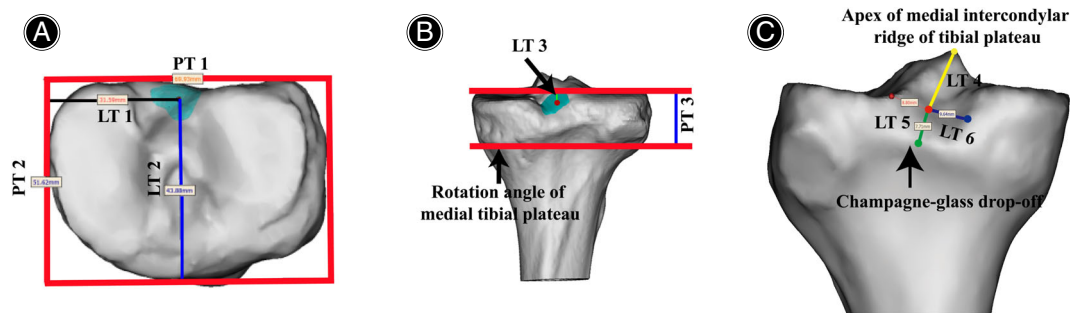


Fig. 5 Measurement of anatomical landmarks around the PCL tibia attachment: (A) LT1 represents the distance from the center of the PCL footprint to the medial edge of the tibial plateau; PT1 represents the width of the tibial plateau; LT2 represents the distance from the center of the PCL footprint to the anterior edge of the tibial plateau; PT2 represents the anterior and posterior diameter of the tibial plateau. (B) LT3 represents the vertical distance from the center to the lowest plane of the tibial plateau; PT3 represents the length of the rotation angle of the tibial plateau to the medial tibial plateau. (C) The bony landmarks of PCL in the fusion images: LT4 represents the distance from apex of medial intercondylar ridge of tibial plateau to the center of PCL footprint in tibia; LT5 represents the distance from champagne-glass drop-off to the center of PCL footprint in tibia. LT6 represents the distance from medial groove to the center of PCL footprint in tibia.

Table 1 The outcomes of the relevant indicators of PCL in femur by the traditional imaging measurement methods in fusion model (mean \pm s)

Indicators	LF1(mm)	LF2(mm)	LF3(mm)	LF1/PF1(%)	LF2/PF2(%)	LF3/PF3(%)
Value	32.1 \pm 1.8	6.8 \pm 2.5	23.3 \pm 2.1	40.6 \pm 2.1	22.5 \pm 8.2	45.3 \pm 4.7

Abbreviations: LF1, The distance from the center of the PCL footprint in femur to the medial border of the medial femoral condyle; LF2, The vertical distance from the center of the PCL footprint in femur to the Blumensaat line; LF3, The distance from the center of the PCL footprint to the anterior cortex of the medial femoral condyle; PCL, Posterior cruciate ligament; PF1, The diameter femoral condyle; PF2, The distance from Blumensaat line to the most distal edge of the medial femoral condyle; PF3, the length of Blumensaat line.

Measurement of Bony Landmarks Surrounding the PCL Tibial Attachment

The peak point of the medial intercondylar ridge of the tibial plateau, the champagne-glass drop-off, and the medial groove were labeled in the fusion model, and the distance from them to the PCL center were measured (LT4, LT5, and LT6, respectively). A schematic diagram of these measurements is presented in Figure 5C.

Statistical Analysis

All data were imported into the SPSS 22.0 software (IBM, Armonk) for statistical analysis. The measurement data are expressed as mean \pm standard deviation (SD). And statistical analysis was performed using paired *t*-tests if the data were normally distributed and satisfied the homogeneity test of variance (Levene's test). A *p* < 0.05 value was considered statistically significant.

Results

Relevant PCL Indicator Identification Via Traditional Image Measurement Methods in the Fusion Model

The PCL footprint data were labeled in the fusion model, using the measurement tool of the Mimics software. In the

femoral footprint attachment, the lengths of LF1-3 were 32.1 \pm 1.8, 6.8 \pm 2.5, and 23.3 \pm 2.1 mm, respectively, and the percentages of LF1/PF1, LF2/PF2, and LF3/PF3 were 40.6% \pm 2.1%, 22.5% \pm 8.2%, and 45.3% \pm 4.7%, respectively. In the tibial attachment, the lengths of LT1-3 were 37.3 \pm 3.3, 45.6 \pm 5.3, and 6.0 \pm 1.2 mm, respectively, and the percentages of LT1/PT1, LT2/PT2, and LT3/PT3 were 50.6% \pm 3.4%, 84.1% \pm 2.9%, and 23.6% \pm 5.2%, respectively. All data are presented in Table 1-2.

The Shape and Area of the PCL Footprint in the Fusion Model

In the fusion image, most femoral PCL attachment footprints were half-moon, fan, or oval shaped, and they extended to the top of the intercondylar fossa. Moreover, the area of the left knee femoral end was measured to be 115.3 \pm 33.5 mm², and the right knee to be 121.8 \pm 35.6 mm². The tibial attachment footprint exhibited a trapezoid shape, characterized by a narrow top and wide bottom, which was mainly located at the posterior half of the PCL slope. The area of the left knee tibial end was also measured to be 146.6 \pm 24.4 mm², and the right knee to be 142.8 \pm 19.5 mm². All data were normally distributed and homogeneous. And no difference was

Table 2 The outcomes of the relevant indicators of PCL in tibia by the traditional imaging measurement methods in fusion model (mean ± s)

Indicators	LT1 (mm)	LT2 (mm)	LT3 (mm)	LT1/PT1 (%)	LT2/PT2(%)	LT3/PT3(%)
Value	37.3 ± 3.3	45.6 ± 5.3	6.0 ± 1.2	50.6 ± 3.4	84.1 ± 2.9	23.6 ± 5.2

Abbreviations: LT1, The distance from the center of the PCL footprint to the medial edge of the tibial plateau; LT2, The distance from the center of the PCL footprint to the anterior edge of the tibial plateau; LT3, The vertical distance from the center to the lowest plane of the tibial plateau; PCL, Posterior cruciate ligament; PT1, The width of the tibial plateau; PT2, The anterior and posterior diameter of the tibial plateau; PT3, The length of the rotation angle of the tibial plateau to the medial tibial plateau.

Table 3 The area of the PCL footprint in fusion image (mm², mean ± s)

	Femur attachment of the footprint	Tibia attachment of the footprint
Left knee	115.3 ± 33.5	146.6 ± 24.4
Right knee	121.8 ± 35.6	142.8 ± 19.5
t Value	0.595	0.544
p Value [†]	0.556	0.560

Abbreviations: PCL: Posterior cruciate ligament.; [†]A paired t-test was used, and $p < 0.05$ means statistically difference.

Table 4 Measurement of relevant bony landmarks around PCL femoral attachment on fusion model (mm, mean ± s)

	LF4	LF5	LF6
Left knee	11.8 ± 2.2	9.5 ± 1.5	18.2 ± 1.8
Right knee	12.1 ± 2.4	10.3 ± 1.8	18.1 ± 2.0
t Value	0.412	1.527	0.166
p Value [†]	0.683	0.135	0.869

Abbreviations: LF4, The distance from apex of the trochlear groove to the center of PCL footprint in femur; LF5, The distance from superficial point to the center of PCL footprint in femur; LF6, The distance from posterior point to the center of PCL footprint in femur; PCL, Posterior cruciate ligament.; [†]A paired t-test was used, and $p < 0.05$ means statistically difference.

observed in the PCL area between the left and right knees ($p = 0.560$). All data are presented in Table 3.

The Bony Landmarks of PCL in the Fusion Images

In the femur, the trochlear, superficial, and posterior points were labeled on the fusion images. The LF4, LF5, and LF6 were measured, and their lengths in the left knee were 11.8 ± 2.2, 9.5 ± 1.5, and 18.2 ± 1.8 mm, respectively, and the corresponding lengths in the right knee were 12.1 ± 2.4, 10.3 ± 1.8, and 18.1 ± 2.0 mm, respectively. All data were normally distributed and homogeneous. There was no

Table 5 Measurement of relevant bony landmarks around PCL tibial attachment on fusion model (mm, mean ± s)

	LT4	LT5	LT6
Left knee	15.3 ± 1.4	9.2 ± 1.8	8.4 ± 2.4
Right knee	16.1 ± 1.8	9.4 ± 2.2	8.0 ± 2.0
t Value	1.569	0.315	0.573
p Value [†]	0.125	0.755	0.570

Abbreviations: LT4, The distance from apex of medial intercondylar ridge of tibial plateau to the center of PCL footprint in tibia; LT5, The distance from champagne-glass drop-off to the center of PCL footprint in tibia; LT6, The distance from medial groove to the center of PCL footprint in tibia; PCL, Posterior cruciate ligament.; [†]A paired t-test was used, and $p < 0.05$ means statistically difference.

statistical difference between the left and right knees for each indicator ($p > 0.05$). All data are presented in Table 4.

In the tibia, the peak point of the medial intercondylar ridge of the tibial plateau, the champagne-glass drop-off, and the medial groove were clearly labeled on the fusion image. The LT4, LT5, and LT6 were measured, and their lengths in the left knee were 15.3 ± 1.4, 9.2 ± 1.8, and 8.4 ± 2.4 mm, respectively, and the corresponding lengths in the right knee were 16.1 ± 1.8, 9.4 ± 2.2 and 8.0 ± 2.0 mm, respectively. All data were normally distributed and homogeneous. There was no statistical difference between the left and right knees for each indicator ($p > 0.05$). All data are presented in Table 5.

Discussion

With the development of arthroscopic techniques, PCL reconstruction is becoming a common treatment strategy for PCL injuries. Precise anatomical positioning of the graft tunnel is essential for obtaining good PCL reconstruction outcomes²¹. However, at present, the positioning of the bone tunnel for PCL reconstruction, under arthroscopic surgery, mainly depends on direct vision and intraoperative imaging positioning during surgery. No matter which intervention is used, there are considerable defects. The direct vision of arthroscopy largely depends on the doctor's experience²². Therefore, it is necessary to establish a knee PCL

imaging model, which can provide more clinically valuable and personalized anatomical information.

Thus, we established the knee joint 3D fusion model based on CT and MRI examination. In the model, the PCL attachment center and relevant bony landmarks which can be easily identified under arthroscopy can be accurately measured. The fusion model can also obtain personalized anatomical data of the PCL on the unaffected side of the patient, and the data is reliable, which can guide clinical PCL reconstruction.

Establishment of the Knee Joint 3D Fusion Model

In order to obtain more reliable anatomical information regarding PCL, multiple researchers reported various methods. Gali and colleagues reported that the PCL bundle's tibial insertions can be identified and marked using metal tags, prior to knee radiography²³. Van Hoof T reported that a contrast medium injected before computed tomography (CT) imaging of the knee can segment and render in 3D imaging, thus, facilitating morphological and morphometric analysis of the PCL²⁴. Although the 3D image can be obtained, the soft tissue of knee, such as ACL, PCL, and meniscus, cannot be shown clearly in CT scan. On the contrary, 3D image of knee joint cannot be obtained by MRI with the advantage showing the soft tissues. In our work, a fusion model that combines both MRI and CT images from the same knee joint was established *via* the MIMICS software, which was shown to overcome the respective deficiencies of MRI or CT imaging alone, and simulated the anatomical shape of the knee joint, including, the femur, tibia, and PCL on MIMICS.

In the model image, the tibia, femur, PCL, meniscus, and cartilage were clearly visualized, and the shape of the PCL femoral end footprint was mostly half-moon shaped, while the tibial footprint area was trapezoidal, which is consistent with the physiological anatomy of the PCL. What's more, the area of the PCL femoral and tibia end footprints was also measured in the fusion model image, and this data was also consistent with the data from prior studies²⁵. All this evidence confirmed that the 3D image can satisfy the anatomical study of PCL.

The Indicators of PCL

It is widely accepted that an accurate determination of the PCL attachment center is key to the success of PCL reconstruction. The most frequently used femoral reference points in recent cadaveric and radiological studies are the anterior cortical border of the medial femoral condyle, the articular cartilage border, and the Blumensaat line. Thus, these landmarks were also measured in the 3D fusion model image, and they were similar to the values of the previous study²⁶. Although accurate positioning of the femoral tunnel during PCL reconstruction is a major factor in restoring knee stability, the incorrect positioning of the tibial tunnel can directly affect stability of the posterior and rotational knee joint²⁷. Thus, the relative tibial

PCL reference point was also investigated. The distance from the PCL tibial footprint center to the medial edge of the tibial plateau, the anterior edge of the tibial plateau, and the lowest plane of the tibial plateau were also measured on the fusion model. This can be highly beneficial for the surgeon to better determine the tibial tunnel of PCL under endoscope.

Bone Landmarks Associated with PCL Attachments

However, it is crucial to ask one question: how will the surgeon determine the center of the PCL footprint area under arthroscopy? There must be certain bone landmarks that can easily be identified under arthroscopy. The 3D fusion model can answer this question. It can obtain the anatomical parameters of a patient's personalized PCL-related markers under arthroscopy, which can be applied toward the reconstruction of the knee joint and during tunnel assessment. The selected reference markers must be measurable under arthroscopy and must also be accurately identified in a fusion image. Therefore, in this study, the trochlear vertex, shallow point (lower point), and posterior point were selected at the femoral site. In addition, the peak point of the medial intercondylar ridge of tibial plateau, the champagne-glass drop-off, and the medial groove were selected at the tibial site. The arthroscopic landmarks selected in this study at the femoral and tibial sites are easily identifiable in fusion images, and we observed no significant variations in the measured data, indicating that these bone landmarks can be employed as a unified positioning reference for PCL reconstruction under arthroscopy. As we all know, there are individual differences in the position, size, and shape of the PCL attachments. Some scholars proposed individualized reconstruction of the PCL in order to restore the anatomical position and biomechanical properties of the PCL to the greatest extent¹⁹. Based on the anatomical symmetry of PCL in both knees, when there is a unilateral disease of the knee joint or the PCL on the affected side lacks a stump for reference, personalized anatomical functional data can be obtained from the unaffected knee joint to specifically guide the anatomical reconstruction and functional rehabilitation of the affected knee joint^{28,29}. Mounting evidence shows that there is no significant difference between the right and left knee on the data of anatomical structures³⁰. Dargel and his colleagues reported that there was a positive correlation in morphometric dimensions between right and left knees in one subject, and there were no significant differences in the morphometric knee joint dimensions between the right and the left knee of a human subject, including PCL-relevant data²⁵. The results of this study support the concept of obtaining PCL morphological reference data from the uninvolved bilateral knee. We demonstrated that our 3D fusion model can obtain personalized anatomical data of the PCL on the unaffected side of the patient, and the data is reliable. Therefore, it is possible to carry out specific measurements of the PCL anatomy of each patient to guide personalized PCL reconstruction.

Strengths and Limitations

This study established a CT-MRI fusion-based three-dimensional model, in which the PCL attachment center and relevant bony landmarks, which can be easily identified under arthroscopy, can be accurately measured. The personalized anatomical data of the PCL on the unaffected side of the patient can be supported in the model, which can play a key role in PCL reconstruction surgery. However, our work encountered certain limitations. First, the radioactivity associated in CT imaging may limit the application of the fusion model. In addition, the high cost of CT and MRI examinations may also limit the popularization and application of the fusion models. Another limitation is that the PCL beam splitting was not examined in the fused image. Although the fusion model can contribute to personalized PCL reconstruction, it cannot be applied to patients who suffer from the diseases of bilateral knee. It is important to note that this research is processed based on healthy people. Thus, the clinical practices are needed to verify the application value of this fusion model. Additionally, our sample size was relatively small. Consequently, a larger sample size is warranted for further investigations to verify the reliability of the fusion model.

Conclusion

In summary, MRI and CT three-dimensional image fusion technology can adequately reconstruct the knee joint, including the PCL. The PCL anatomical data, measured on our model, is highly reliable and can guide clinical PCL reconstruction. Additionally, the PCL-related landmarks can be

recognized and measured in fusion MRI and CT images under arthroscopy. This can potentially guide PCL reconstruction by locating tunnels accurately under arthroscope.

Acknowledgements

The authors would like to thank all the reviewers who participated in the review, as well as MJEditor (www.mjeditor.com) for providing English editing services during the preparation of this manuscript.

Author Contributions

Conceptualization, W.M.W.; Methodology, W.M.W., K.Y.F.; Investigation, T.Y.W., X.R.H., M.X.J.M., J.T., and Z.A.Q.; Formal Analysis, K.Y.F. and T.Y.W.; Resources, K.Y.F. and T.Y.W.; Writing - Original Draft, K.Y.F. and T.Y.W.; Writing—Review and Editing, K.Y.F., T.Y.W., and J.T.; Visualization, W.M.W.; Supervision, W.M.W.

Disclosure Statement

The authors declared no conflicts of interest.

Ethics Statement

All procedures were reviewed and approved by the hospital ethics committee and are in accordance with the Declaration of Helsinki, and all volunteers signed an informed consent form.

Funding Information

None.

Reference

- Nedopil AJ, Howell SM, Hull ML. More passive internal tibial rotation with posterior cruciate ligament retention than with excision in a medial pivot TKA implanted with unrestricted caliper verified kinematic alignment. *Knee Surg Sports Traumatol Arthrosc.* 2021.
- Ahn DY, Park HJ, Kim MS, Kim JN, Hong SW, Kim E, et al. Protruding anterior medial meniscus and posterior tibial translation as secondary signs of complete and partial posterior cruciate ligament tear. *Br J Radiol.* 2022;95(1133):20210976.
- Qi H, Lu Y, Li M, Ren C, Xu Y, Ma T, et al. Open reduction and internal fixation of the tibial avulsion fracture of the posterior cruciate ligament: which is better, a hollow lag screw combined with a gasket or a homemade hook plate? *BMC Musculoskelet Disord.* 2022;23(1):143.
- Owesen C, Sandven-Thrane S, Lind M, Forssblad M, Granan LP, Årøen A. Epidemiology of surgically treated posterior cruciate ligament injuries in Scandinavia. *Knee Surg Sports Traumatol Arthrosc.* 2017;25(8):2384–91.
- Winkler PW, Zsidai B, Wagala NN, Hughes JD, Horvath A, Senorski EH, et al. Evolving evidence in the treatment of primary and recurrent posterior cruciate ligament injuries, part 2: surgical techniques, outcomes and rehabilitation. *Knee Surg Sports Traumatol Arthrosc.* 2021;29(3):682–93.
- Brisson NM, Agres AN, Jung TM, Duda GN. Gait adaptations at 8 years after reconstruction of unilateral isolated and combined posterior cruciate ligament injuries. *Am J Sports Med.* 2021;49(9):2416–25.
- Tucker CJ, Cotter EJ, Waterman BR, Kilcoyne KG, Cameron KL, Owens BD. Functional outcomes after isolated and combined posterior cruciate ligament reconstruction in a military population. *Orthop J Sports Med.* 2019;7(10):2325967119875139.
- Yoon KH, Bae DK, Song SJ, Cho HJ, Lee JH. A prospective randomized study comparing arthroscopic single-bundle and double-bundle posterior cruciate ligament reconstructions preserving remnant fibers. *Am J Sports Med.* 2011;39(3):474–80.
- Song EK, Park HW, Ahn YS, Seon JK. Transtibial versus tibial inlay techniques for posterior cruciate ligament reconstruction: long-term follow-up study. *Am J Sports Med.* 2014;42(12):2964–71.
- Kim MS, Park HJ, Kim JN, Jeon MR, Kim E, Park JH, et al. Postsurgical status of articular cartilage after arthroscopic posterior cruciate ligament reconstruction in patients with or without concomitant meniscal pathology. *Clin Imaging.* 2021;80:406–12.
- Kernkamp WA, Jens AJT, Varady NH, van Arkel ERA, Nelissen R, Asnis PD, et al. Anatomic is better than isometric posterior cruciate ligament tunnel placement based upon in vivo simulation. *Knee Surg Sports Traumatol Arthrosc.* 2019;27(8):2440–9.
- Korthaus A, Krause M, Pagenstert G, Warncke M, Brembach F, Frosch KH, et al. Tibial slope in the posterolateral quadrant with and without ACL injury. *Arch Orthop Trauma Surg.* 2021.
- Dong C, Zhao C, Li M, Fan C, Feng X, Piao K, et al. Accuracy of tibial tuberosity-trochlear groove distance and tibial tuberosity-posterior cruciate ligament distance in terms of the severity of trochlear dysplasia. *J Orthop Surg Res.* 2021;16(1):383.
- Teng Y, Da L, Jia G, Hu J, Liu Z, Zhang S, et al. What is the maximum Tibial tunnel angle for Transtibial PCL reconstruction? A comparison based on virtual radiographs, CT images, and 3D knee models. *Clin Orthop Relat Res.* 2022;480:918–28.
- Salim R, Salzler MJ, Bergin MA, Zheng L, Carey RE, Kfuri M Jr, et al. Fluoroscopic determination of the tibial insertion of the posterior cruciate ligament in the sagittal plane. *Am J Sports Med.* 2015;43(5):1142–6.
- Araujo PH, Moloney G, Rincon G, Carey R, Zhang X, Harner C. Use of a fluoroscopic overlay to guide femoral tunnel placement during posterior cruciate ligament reconstruction. *Am J Sports Med.* 2014;42(11):2673–9.
- Greiner P, Magnussen RA, Lustig S, Demey G, Neyret P, Servin E. Computed tomography evaluation of the femoral and tibial attachments of the posterior cruciate ligament in vitro. *Knee Surg Sports Traumatol Arthrosc.* 2011;19(11):1876–83.
- Park HJ, Lee SY, Choi SH, Ahn JH, Park SJ, Park JH, et al. Comparison of oblique coronal images in knee of three-dimensional isotropic T(2)-weighted turbo spin echo MRI versus two-dimensional fast spin echo T(2)-weighted sequences

for evaluation of posterior cruciate ligament injury. *Br J Radiol.* 2016;89(1067):20160554.

- 19.** Scanlan SF, Lai J, Donahue JP, Andriacchi TP. Variations in the three-dimensional location and orientation of the ACL in healthy subjects relative to patients after transtibial ACL reconstruction. *J Orthop Res.* 2012;30(6):910–8.
- 20.** Dong Y, Mou Z, Huang Z, Hu G, Dong Y, Xu Q. Three-dimensional reconstruction of subject-specific knee joint using computed tomography and magnetic resonance imaging image data fusions. *Proc Inst Mech Eng H.* 2013;227(10):1083–93.
- 21.** Yoon KH, Kim JS, Park JY, Park SY, Kiat RYD, Kim SG. Comparable clinical and radiologic outcomes between an anatomic tunnel and a low Tibial tunnel in remnant-preserving posterior cruciate ligament reconstruction. *Orthop J Sports Med.* 2021;9(2):2325967120985153.
- 22.** Tachibana Y, Tanaka Y, Kinugasa K, Mae T, Horibe S. Tunnel enlargement correlates with postoperative posterior laxity after double-bundle posterior cruciate ligament reconstruction. *Orthop J Sports Med.* 2021;9(1):2325967120977834.
- 23.** Gali JC, Esquerdo P, Almagro MA, da Silva PA. Radiographic study on the tibial insertion of the posterior cruciate ligament. *Rev Bras Ortop.* 2015;50(3):342–7.
- 24.** Van Hoof T, Cromheecke M, Tampere T, D'Herde K, Victor J, Verdonk PC. The posterior cruciate ligament: a study on its bony and soft tissue anatomy using

novel 3D CT technology. *Knee Surg Sports Traumatol Arthrosc.* 2013;21(5):1005–10.

- 25.** Dargel J, Feiser J, Gotter M, Pennig D, Koebke J. Side differences in the anatomy of human knee joints. *Knee Surg Sports Traumatol Arthrosc.* 2009;17(11):1368–76.
- 26.** Johannsen AM, Anderson CJ, Wijdicks CA, Engebretsen L, LaPrade RF. Radiographic landmarks for tunnel positioning in posterior cruciate ligament reconstructions. *Am J Sports Med.* 2013;41(1):35–42.
- 27.** Gill TJ, DeFrate LE, Wang C, Carey CT, Zayontz S, Zarins B, et al. The effect of posterior cruciate ligament reconstruction on patellofemoral contact pressures in the knee joint under simulated muscle loads. *Am J Sports Med.* 2004;32(1):109–15.
- 28.** Sonnery-Cottet B, Archbold P, Thauat M, de Oliveira Alves Tostes MD, Besse JL. Fifth toe plantar plate repair in a professional soccer player: case report. *Foot Ankle Int.* 2012;33(7):598–601.
- 29.** Li G, Papannagari R, Li M, Bingham J, Nha KW, Allred D, et al. Effect of posterior cruciate ligament deficiency on in vivo translation and rotation of the knee during weightbearing flexion. *Am J Sports Med.* 2008;36(3):474–9.
- 30.** Chen Y, Ding J, Dai S, Yang J, Wang M, Tian T, et al. Radiographic measurement of the posterior tibial slope in normal Chinese adults: a retrospective cohort study. *BMC Musculoskelet Disord.* 2022;23(1):386.